Can Point Defects in Surfaces in Solution be Atomically Resolved by Atomic Force Microscopy?

Bernhard Reischl,* Paolo Raiteri, Julian D. Gale, and Andrew L. Rohl
Curtin Institute for Computation and Department of Chemistry,
Curtin University, GPO Box 1987, Perth, Western Australia, 6845, Australia
(Dated: 15 October 2016)

While the atomic force microscope (AFM) is able to image mineral surfaces in solution with atomic resolution, so far it has been a matter of debate whether imaging point defects is also possible under these conditions. The difficulties stem from the limited knowledge of what types of defects may be stable in the presence of an AFM tip, as well as from the complicated imaging mechanism involving interactions between hydration layers over the surface and around the tip apex. Here, we present atomistic molecular dynamics and free energy calculations of the AFM imaging of vacancies and ionic substitutions in the calcite ($10\bar{1}4$) surface in water, using a new silica AFM tip model. Our results indicate that both calcium and carbonate vacancies, as well as a magnesium substitution, could be resolved in an AFM experiment, albeit with different imaging mechanisms.

The atomic force microscope (AFM) [1] can be used to study surfaces in solution in real space with atomic resolution [2, 3] and has become an indispensable tool in understanding hydration [4–7], crystal growth and dissolution [8–10]. In pioneering work by the inventors of the AFM, contact mode in humid air produced images with the lattice periodicity of the calcite basal plane across several monosteps [11]. However, true atomic resolution in liquid [2, 3] and ambient conditions [12] was only achieved later using dynamic AFM modes [13], where the tip is oscillated during the scan, and the changes in resonant frequency, amplitude, or phase are recorded [2, 14, 15]. While the ability to resolve atomic-scale defects in a periodic surface is the ultimate proof of *atomic resolution*, the ability to reliably image defects and their dynamics would considerably improve our understanding of surface processes in solution, and enable the study of growth or dissolution of minerals in solution at the atomistic level.

Thanks to recent advances in AFM technology, it is now possible to obtain images or movies containing isolated imperfections in a periodic structure [16, 17]. However, these experimental studies have not been able to interpret what they have observed, due to the lack of knowledge regarding the imaging mechanism. The stability and dynamics of surface defects can be very different at the interface with a liquid, compared to vacuum, because most processes will be mediated by the solvent molecules, and potentially even solutes, especially for charged defects. Even less is known regarding the specific water-mediated interaction mechanism between surface defects and the AFM tip.

Many breakthroughs in AFM have only been achieved alongside sophisticated simulations to ensure the images are interpreted correctly, such as the differentiation of chemical bonds in individual molecules *in vacuo* by Gross et al. [18]. Atomic-scale imaging paired with computational modeling of the AFM model tip interacting with surface defects in vacuum is well established and has furthered our understanding of surfaces and interfacial processes [19, 20]. At the solid-liquid interface, the situation is naturally more complicated, especially for ionic crystal surfaces that exhibit well-defined hydration layers. Here, the oscillating AFM tip is not only interacting with the surface atoms, but also with the ordered water molecules in the hydration layers above it.

Recent developments in the simulation of AFM in liquid, based on atomistic simulations and free energy calculations, have made it possible to determine the imaging mechanism of ionic crystal surfaces and their hydration layers in solution [21–23]. In the present study, we build on this methodology to investigate the imaging mechanism of point defects in surfaces in solution from a theoretical point of view. We chose the calcite ($10\bar{1}4$) cleavage plane as our model surface, because of its importance in surface science and biomineralization, and as a benchmark system for studying crystal growth by AFM [24]. We consider both calcium and carbonate ion vacancies, as well as a substitution of a calcium ion with a magnesium ion, commonly found in geological samples [25].

The stability of calcite ($10\bar{1}4$) surfaces with point defects, and the changes in surface and hydration layer structure around the defects were investigated using molecular dynamics simulations. The atomistic interactions between the mineral surface and water were described by the force field developed by Raiteri et al. [26], using the SPC/Fw potential for water [27]. The force field was parametrized to reproduce both the structure and thermodynamics of the mineral phases of $CaCO_3$, as well as the thermodynamics of the ions in solution, and is therefore believed to accurately describe the solid-liquid interface [28]. The hydration layer structure at the calcite-water interface is shown in Figs. 1(a) and 1(b). For the surfaces with vacancies, we removed an ion of the opposite charge from the opposite surface of the slab to ensure charge neutrality of the simulation cell. This effectively introduces a dipole across the calcite slab. However, we observed no breaking of the symmetry of the

hydration layer structures on either side of the slab, beyond those changes clearly due to the presence of the defect, and therefore consider the effect of the dipole to be negligible.

For the AFM simulation, we proceeded in two steps. First, free energy calculations were performed with an AFM tip model on a rectangular 8×4 grid over one unit cell of the perfect surface and, after assessing the lateral extent of the changes induced by the presence of each defect, similar calculations were performed over an appropriate area around the defects, on a grid with the same spacing. The setup for the AFM simulation is shown in Fig. 1(c), and uses a silica tip. This is expected to be a reasonable model of the apex of a silicon (or silicon nitride) AFM tip, covered in several nanometers of native oxide, that has reacted with water to form silanol groups [29, 30], and has not been covered in surface material from initial contact with the sample [31, 32]. The tip was constructed from bulk β-cristobalite, and all broken Si–O bonds on the surface were replaced by silanol groups (Si–OH), with a sharp termination in a single silanol group at the apex. The interactions between SiO_2/SiOH and water were described by the ClayFF forcefield [33], and parameters for the direct interactions with the calcite surface were either constructed from combination rules, or by analogy to the interactions of calcite with the OH group in bicarbonate (Additional information on the silica tip hydration structure can be found in the Supplemental Material. A more detailed comparison of the performance of simulated AFM images obtained with our different tip models [23, 34, 35] in comparison to experiment will be published elsewhere [36].)

Here we used the LAMMPS molecular dynamics code [37] in conjunction with the PLUMED plugin [38] to perform umbrella sampling of the free energy profiles of the system as a function of the tip-surface separation distance. We used the z component of the center of mass distance between the top of the silica nanocluster and the calcite slab as a collective variable (CV), z_C, as illustrated in Fig. 1(c). Harmonic restraints were applied on the top of the tip along x and y, to avoid lateral drift or rotation. Similar restraints were applied on the fourth layer from the bottom of the calcite slab along x, y, and z, to anchor it in the frame of reference of the simulation box. The starting configurations for the umbrella windows were obtained from preliminary steered MD runs, where the tip was dragged towards the surface along the same CV, and configurations were saved every 0.05 nm, in the range $2.30 \leq z_C \leq 3.85$ nm. This corresponds to a range of tip-surface separation distances, z, from over 1 nm down to hard contact. The umbrella potential had a force constant of 0.5 eV/Å^2, and the distributions of the CV were obtained from 7 ns of sampling, after 1 ns equilibration and decorrelation from the starting configuration. The free energy profiles were obtained with the WHAM code [39]. All simulations were carried out in the

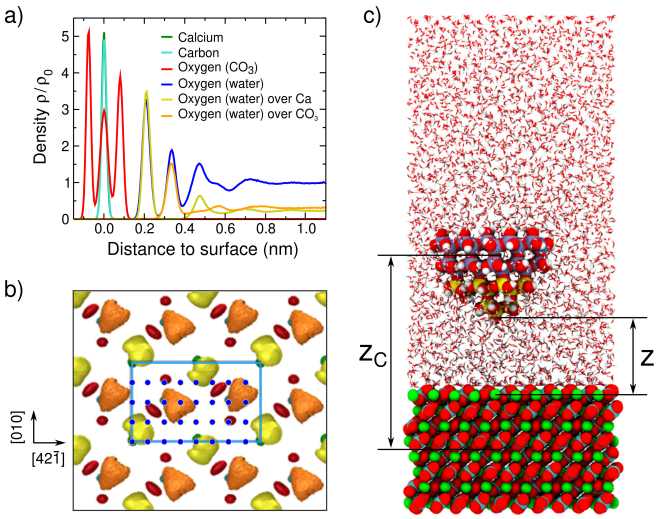

FIG. 1. Calcite hydration structure: atomic number densities, relative to the density of bulk water ρ_0, along the perpendicular to the surface (a), and density isosurface plots at the non-defective calcite surface (b). Calcium is green, carbon cyan, carbonate oxygen red. The water density isosurfaces in the first layer over calcium and the second layer over carbonate are yellow and orange, respectively. The isosurface values are $10\rho_0$ for the calcite atoms and $4\rho_0$ for water. The calcite surface unit cell, measuring 0.809×0.494 nm^2, is indicated by a blue rectangle, and the 8×4 grid points for the free energy calculation with the AFM tip are marked by blue dots. For the AFM simulation, the system consists of a calcite slab eight layers thick, exposing the $(10\bar{1}4)$ surface along z, the silica AFM tip model, and water (c). Here, silicon atoms are colored in yellow, oxygen in red, and hydrogen in white, and the silicon atoms in the upper part of the tip which is used for the definition of the collective variable z_C are highlighted in light blue.

NVT ensemble, with a Nosé-Hoover chain thermostat of length 5 and time constant 0.1 ps maintaining the temperature at 300 K. Long-ranged electrostatic interactions were treated with the PPPM scheme, using a real space cutoff of 0.9 nm and an accuracy of 10^{-5}.

In the second step, we computed the effective 3D force field for the tip from the derivative of the free energy profiles with respect to z_C, interpolating laterally along x and y using a cubic spline. For the systems with defects, the force curves obtained around the defect were embedded in the periodically repeated 32 curves obtained on the perfect surface. These three effective force fields, one for each defect, were subsequently used in virtual frequency modulation AFM (FM-AFM) simulations using the PyVAFM code [40], to simulate 2D scan images in x-y planes, with a cantilever of resonant frequency 150 kHz, spring constant 50 N/m, oscillation amplitude 0.2 nm, and a Q-factor of 10, similar to probes commonly used in experiment [3]. While the last step is computationally very inexpensive, carrying out the free energy calculations to construct the effective force fields required over

5×10^6 CPU hours.

Our simulations showed that all three systems with defects equilibrated in 1–2 ns and remained stable for the duration of the 50 ns MD trajectory, even without local charge compensation through a hydronium, hydroxide, or other counter ion from solution, which would likely occur in a real system with charged vacancies.

The time-averaged atomic densities at the interface around the three defect sites, shown in Fig. 2, indicate that the changes in the surface around the vacancies are limited to an area of approximately one surface unit cell, and are more pronounced for the calcium vacancy, where a rotation of the surrounding four carbonate ions is clearly visible. In the case of both types of vacancies, water molecules are present in the cavity, and occupy equilibrium positions that allow hydrogen bonding with water molecules in the hydration layers above, as well as with ions in the surface and subsurface layer. This also leads to a perturbation of the equilibrium structure in the first and second hydration layers. While the analysis of the MD trajectory identifies equilibrium sites for water molecules in the cavity, this equilibrium is highly dynamic with multiple exchanges on the nanosecond time scale. However, the increased coordination of ions around the vacancy by water molecules in the cavity did not lead to dissolution on the time scale of the simulations. The changes in hydration layer structure affect a larger area around the vacancies than the distortions in the crystal surface of up to 2×2 surface unit cells.

In contrast to the vacancies, the charge neutral magnesium substitution induces very little change in the positions of the neighboring calcium and carbonate ions. The changes in the hydration layer geometry are also more subtle; the lateral order in the hydration layers is unaffected, but due to the smaller ionic radius and larger solvation free energy of Mg^{2+} compared to Ca^{2+}, the water density maximum in the first hydration layer above the magnesium ion is shifted by ~ 0.03 nm closer to the surface.

For all three defects, the most visible deviations from the hydration layer structure over the perfect surface are found directly above the defects and their neighbouring ions. Based on the changes in surface and hydration layer structures shown in Fig. 2, we deemed it sufficient to recalculate the free energy profiles for the AFM tip only over 5×5 grid points centred on the magnesium substitution, and 8×7 grid points around the two vacancies.

In Fig. 3(a), the force-distance curves obtained with the silica tip over the perfect calcite surface unit cell indicate the possibility of atomic scale contrast and qualitatively present the same minima and maxima as those obtained with a calcite tip model in previous work [23], as shown in the Supplementary Material. The 1D force profiles over the defect compared to the equivalent occupied site in the perfect surface, as well as the 2D force maps obtained from slices through the full 3D force maps parallel (xy) and perpendicular (xz) to the surface (Fig. 3 (b) and (c)), indicate tip-surface distances at which the AFM tip might be sensitive to the defect, keeping in mind that the imaging mechanism can be indirect, i.e. the contrast may be caused by the changes in the hydration layers above the defect.

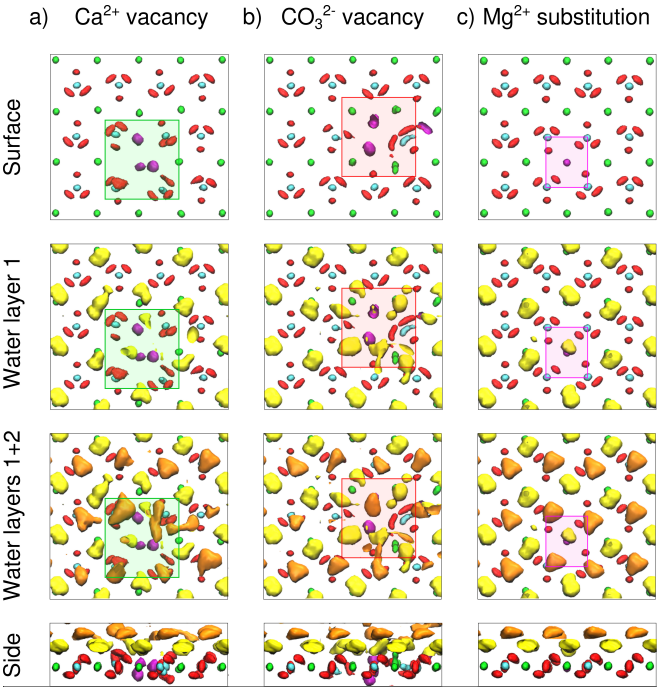

FIG. 2. Changes in surface and hydration layer structure in calcite surfaces with a calcium ion vacancy (a), a carbonate ion vacancy (b) and a magnesium substitution (c). The colors and density values of the isosurface maps are the same as in the image of the perfect surface in Fig. 1b, and magnesium is shown in magenta and water molecules inside the cavity of the vacancies in purple. The green, red, and magenta rectangles indicate where free energy profiles were collected around the defects in the subsequent AFM simulation.

The simulated AFM frequency shift images (Fig. 3(d)) look very similar to the 2D cross-sections through the 3D force map obtained from the free energy calculations when the lower turning point of the tip oscillation is close to the height of the 2D force map. However, small differences can be expected, because in the AFM simulation the signal is averaged over the entire tip oscillation range. This highlights the importance of the second step in the simulation approach, if a direct comparison to experiment is intended.

All three defects can be imaged as a 'dark spot' at a position where a 'bright spot' should be seen in the perfect surface, in a certain tip-surface distance range. In terms of the imaging mechanism, we find that both the calcium vacancy and the magnesium substitution exhibit this attenuated contrast when the tip is imaging the first hydration layer over the calcium sub-lattice; over the calcium vacancy, the hydration structure is perturbed, and

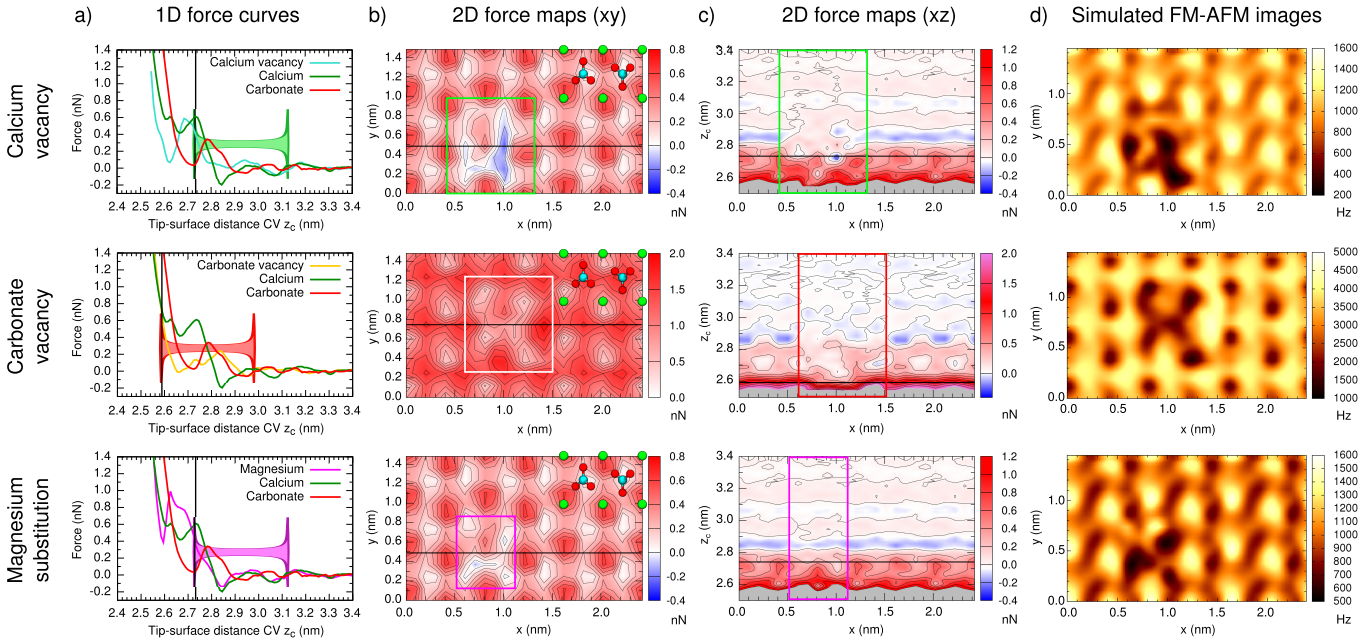

FIG. 3. 1D force-distance curves (a), 2D force maps parallel (b) and perpendicular to the surface (c), and simulated FM-AFM images (d) over a calcium vacancy (top), carbonate vacancy (centre), and magnesium substitution (bottom). The distances for the 2D xy force maps were chosen according to the best contrast of the defect that could be observed, and are marked by vertical black lines in the force-distance curve plots. The corresponding simulated frequency shift images were obtained with the tip oscillating in the ranges indicated by the colored bar in the force-distance curve plots. The width of the bar is proportional to the time spent by the cantilever at a given distance. The 2D xz force maps, perpendicular to the surface, taken at the position of the horizontal black line in the 2D xy force maps emphasize the differences in force contrast over the different defects. The rectangles in the 2D force maps delimit the data obtained from simulations on surfaces with defects.

the tip feels less repulsion compared to the equivalent site in the perfect surface. Over the magnesium substitution, the first hydration layer water molecule is found at the same lateral position as over calcium, but at a lower z position, which is sufficient to cause a contrast of similar magnitude as for the calcium vacancy. In fact, the simulated AFM images over the calcium vacancy and magnesium substitution are very similar. However, as can be seen in the force maps in (x,z) planes (Fig. 3(c)), upon reducing the tip-surface distance over the Mg^{2+} substitution, the contrast changes, and then the water molecule appears as a 'bright spot' – a feature missing over the calcium vacancy, which could be used to distinguish between the two types of defect. These findings also suggest the possibility to resolve the rows of Ca and Mg ions in $(10\bar{1}4)$ surfaces of dolomite $[CaMg(CO_3)_2]$.

The carbonate vacancy is only observed clearly when the tip is interacting directly with the surface at the lower turning point, i.e. in the strongly repulsive regime with forces exceeding 1 nN. At this tip-surface distance, the first hydration layer has been displaced and the tip experiences a stronger repulsion over the carbonate groups than the calcium ions, which is mainly due to the electrostatic repulsion between the negatively charged carbonate ion oxygen and the silanol hydroxyl group at the tip apex. Over the vacancy, which still contains two water molecules, this repulsion is weaker, causing the contrast. The calcium vacancy is not visible when the tip interacts directly with the surface. However, which vacancy is imaged at this distance will strongly depend on the charge of the tip apex.

At some tip positions, we observed larger displacement of one or two ions adjacent to the vacancies than in the simulations without tip, but no dissolution events or defect migration occurred on the timescale of simulations and no correlation between ion displacement from around the vacancies and tip position could be established. Indeed, a likely reason why we observe infrequent larger displacements of ions in the simulations with the tip is statistical in nature: the combined simulation times with and without the tip are 6.4 μs and 50 ns, respectively (see detailed analysis in the Supplemental Material). We also note that the vacancies, although charged by $\pm 2e$, only interact significantly with the tip at distances below 1 nm, due to the strong screening by the water molecules.

Our simulations indicate that FM-AFM with a conventional cantilever for imaging in liquid should be able to atomically resolve both calcium and carbonate vacancies in calcite–provided these are stable in a real surface–and a substitution of a divalent cation with a different

solvation shell, such as Mg^{2+} and quite possibly Fe^{2+}, which are commonly found in geological samples of calcite. However, the imaging mechanisms are found to be different; while the calcium vacancy and magnesium substitution are imaged as a change in the first hydration layer, the carbonate vacancy is only resolved when the tip is interacting with the surface atoms directly. We hope this result encourages AFM experimentalists to apply recent advances in methodology, such as the possibility to acquire 3D data sets of the interfacial volume [41, 42], to the study of atomic-scale defects in mineral surfaces in solution. Together with help from simulation, a proper identification of such defects should then be possible, and enable further studies of surface processes where defects play an important role, such as growth and dissolution, or biomineralization.

This work has been supported by the Australian Research Council Discovery Programme (DP 140101776 and FT 130100463). We are indebted to the Australian Government and the Government of Western Australia for providing computational resources through the Pawsey Supercomputing Centre under the National Computational Merit Allocation Scheme. We thank John Tracey and Peter Spijker (Aalto University), Matthew Watkins (University of Lincoln), and Alexander L. Shluger (University College London) for useful discussions.

* bernhard.reischl@curtin.edu.au

[1] G. Binnig, C. F. Quate, and C. Gerber, Phys. Rev. Lett. **56**, 930 (1986).
[2] T. Fukuma, K. Kobayashi, K. Matsushige, and H. Yamada, Appl. Phys. Lett. **87**, 034101 (2005).
[3] S. Rode, N. Oyabu, K. Kobayashi, H. Yamada, and A. Kühnle, Langmuir **25**, 2850 (2009).
[4] J. P. Cleveland, T. E. Schäffer, and P. K. Hansma, Phys. Rev. B **52**, 8692 (1995).
[5] T. Fukuma, M. J. Higgins, and S. P. Jarvis, Biophys. J. **92**, 3603 (2007).
[6] J. I. Kilpatrick, S.-H. Loh, and S. P. Jarvis, J. Am. Chem. Soc. **135**, 2628 (2013).
[7] Y. Araki, K. Tsukamoto, R. Takagi, T. Miyashita, N. Oyabu, K. Kobayashi, and H. Yamada, Cryst. Growth Des. **14**, 6254 (2014).
[8] G. T. Paloczi, B. L. Smith, P. K. Hansma, D. A. Walters, and M. A. Wendman, Appl. Phys. Lett. **73**, 1658 (1998).
[9] K. Miyata, H. Asakawa, and T. Fukuma, Appl. Phys. Lett. **103**, 203104 (2013).
[10] F. Jones and M. I. Ogden, CrystEngComm **12**, 1016 (2010).
[11] F. Ohnesorge and G. Binnig, Science **260**, 1451 (1993).
[12] D. S. Wastl, A. J. Weymouth, and F. J. Giessibl, ACS Nano **8**, 5233 (2014).
[13] R. García and R. Perez, Surf. Sci. Rep. **47**, 197 (2002).
[14] A. Labuda, J. Cleveland, N. A. Geisse, M. Kocun, B. Ohler, R. Proksch, M. B. Viani, and D. Walters, Microscopy and Analysis **28**, S21 (2014).
[15] T. Fukuma, J. I. Kilpatrick, and S. P. Jarvis, Rev. Sci. Instrum. **77**, 123703 (2006).
[16] I. Siretanu, D. van den Ende, and F. Mugele, Nanoscale **8**, 8220 (2016).
[17] S. Hofmann, K. Voïtchovsky, P. Spijker, M. Schmidt, and T. Stumpf, Sci. Rep. **6**, 21576 (2016).
[18] L. Gross, F. Mohn, N. Moll, B. Schuler, A. Criado, E. Guitian, D. Pena, A. Gourdon, and G. Meyer, Science **337**, 1326 (2012).
[19] W. A. Hofer, A. S. Foster, and A. L. Shluger, Rev. Mod. Phys. **75**, 1287 (2003).
[20] A. S. Foster, O. H. Pakarinen, J. M. Airaksinen, J. D. Gale, and R. M. Nieminen, Phys. Rev. B **68**, 195410 (2003).
[21] M. Watkins and A. L. Shluger, Phys. Rev. Lett. **105**, 196101 (2010).
[22] M. Watkins, M. L. Berkowitz, and A. L. Shluger, Phys. Chem. Chem. Phys. **13**, 12584 (2011).
[23] T. Fukuma, B. Reischl, N. Kobayashi, P. Spijker, F. F. Canova, K. Miyazawa, and A. S. Foster, Phys. Rev. B **92**, 155412 (2015).
[24] E. Ruiz Agudo and C. V. Putnis, Mineral. Mag. **76**, 227 (2012).
[25] A. O. Harstad and S. L. S. Stipp, Geochim. Cosmochim. Acta **71**, 56 (2007).
[26] P. Raiteri, R. Demichelis, and J. D. Gale, J. Phys. Chem. C **119**, 24447 (2015).
[27] Y. Wu, H. L. Tepper, and G. A. Voth, J. Chem. Phys. **124**, 024503 (2006).
[28] P. Fenter, S. Kerisit, P. Raiteri, and J. D. Gale, J. Phys. Chem. C **117**, 5028 (2013).
[29] L. T. Zhuravlev, Colloids Surf., A **173**, 1 (2000).
[30] M.-H. Du, A. Kolchin, and H.-P. Cheng, J. Chem. Phys. **119**, 6418 (2003).
[31] D. Argyris, A. Phan, A. Striolo, and P. D. Ashby, J. Phys. Chem. C **117**, 10433 (2013).
[32] S. M. R. Akrami, H. Nakayachi, T. Watanabe-Nakayama, H. Asakawa, and T. Fukuma, Nanotechnology **25**, 455701 (2014).
[33] R. T. Cygan, J.-J. Liang, and A. G. Kalinichev, J. Phys. Chem. B **108**, 1255 (2004).
[34] B. Reischl, M. Watkins, and A. S. Foster, J. Chem. Theory Comput. **9**, 600 (2013).
[35] M. Watkins and B. Reischl, J. Chem. Phys. **138**, 154703 (2013).
[36] T. Fukuma, K. Miyazawa, B. Reischl, P. Raiteri, J. Tracey, P. Spijker, J. D. Gale, A. L. Rohl, and A. S. Foster, (2016), in preparation.
[37] S. Plimpton, J. Comp. Phys. **117**, 1 (1995), http://lammps.sandia.gov.
[38] G. A. Tribello, M. Bonomi, D. Branduardi, C. Camilloni, and G. Bussi, Comput. Phys. Commun. **185**, 604 (2014).
[39] A. Grossfield, WHAM: the weighted histogram analysis method, version 2.0.9, http://membrane.urmc.rochester.edu/content/wham.
[40] J. Tracey, F. F. Canova, O. Keisanen, D. Z. Gao, P. Spijker, B. Reischl, and A. S. Foster, Comput. Phys. Commun. **196**, 429 (2015).
[41] T. Fukuma, Y. Ueda, S. Yoshioka, and H. Asakawa, Phys. Rev. Lett. **104**, 016101 (2010).
[42] C. Marutschke, D. Walters, J. Cleveland, I. Hermes, R. Bechstein, and A. Kühnle, Nanotechnology **25**, 335703 (2014).